Colloids and Surfaces B: Biointerfaces 130 (2015) 237–245

Contents lists available at ScienceDirect

Colloids and Surfaces B: Biointerfaces

journal homepage: www.elsevier.com/locate/colsurfb

Stable self-assembled nanostructured hen egg white lysozyme exhibits strong anti-proliferative activity against breast cancer cells

Sailendra Mahanta[a], Subhankar Paul[a,*], Ankit Srivastava[b], Ashutosh Pastor[b], Bishwajit Kundu[b], Tapan K. Chaudhuri[b]

[a] Structural Biology and Nanomedicine Laboratory, Department of Biotechnology and Medical Engineering, National Institute of Technology, Rourkela 769008, Odisha, India
[b] Kusuma School of Biological Sciences, Indian Institute of Technology Delhi, New Delhi 110016, India

ARTICLE INFO

Article history:
Received 22 January 2015
Received in revised form 4 April 2015
Accepted 8 April 2015
Available online 17 April 2015

Keywords:
Self-assembled nanostructured lysozyme
Breast cancer
Circular dichroism
Fluorescence spectroscopy
MTT assay
Cytoplasmic granules

ABSTRACT

Chemotherapy side effects have long been a matter of great concern. Here we describe a structurally stable self-assembled nanostructured lysozyme (snLYZ) synthesized using a simple desolvation technique that exhibited anticancer activity, as well as excellent hemocompatibility. Field emission scanning electron microscopy; atomic force microscopy and dynamic particle size analyzer were used for analyzing the synthesized snLYZ. The analysis revealed spherical shape with an average size of 300 nm. Circular dichroism and tryptophan fluorescence spectroscopic analysis revealed its gross change in secondary as well as the tertiary level of the structure. snLYZ also demonstrated excellent structural as well as the functional stability of LYZ in a wide range of pH and temperature with a fair level of protection against proteinase K digestion. When applied to MCF-7 breast cancer cells, it exhibited approximately 95% cell death within 24 h, involving a reactive oxygen species (ROS) based mechanism, and showed excellent hemocompatibility. Fluorescence microscopy imaging revealed distinct cellular internalization of snLYZ and the formation of cytoplasmic granules, which initiated a cell-killing process through membrane damage. In order to mimic targeted therapy, we tagged folic acid with snLYZ, which further enhanced cytotoxicity against MCF-7 cells. Therefore, this is the first report of its kind where we demonstrated the preparation of a highly stable self-assembled nanostructured lysozyme with a strong anti-proliferative activity against breast cancer cells.

1. Introduction

Proteins are highly sensitive to external stress because of their intimate link between 3-D structure and biological function [1–3]. Proteins also possess unique properties to form self-assembled nanostructures. They form disordered as well as ordered aggregates in cells. In many instances, such accumulation is the cause of number of lethal diseases like Amyloidosis, Alzheimer's, Parkinson's and Prion disease [4–7]. However, protein structure and their self-assembly process are externally driven and has found many applications in biology and medicine [8–15]. Nanoparticles, developed from natural biopolymers are usually biodegradable, easy to metabolize, and easily surface modifiable, which may facilitate efficient attachment of drugs [16]. Such nanoparticles have been reported to develop from various proteins including bovine and human serum albumin, zein and gliadin [16].

Recent reports cite special preparation of small proteins such as bovine and human α-lactalbumin, to be lethal against a number of tumor cell types. Specific conformational state of proteins was also reported to form conjugates with oleic acid known as BAMLET (Bovine α-lactalbumin made lethal to tumor cells) or HAMLET (Human α-lactalbumin made lethal to tumor cells). These conjugates also induced tumor cell death [17,18]. Therefore, specific structural state of such proteins may have a therapeutic potential.

Here we report the use of hen egg white lysozyme (LYZ) for the preparation of self-assembled nanostructured lysozyme (snLYZ). Breast cancer cells were treated with snLYZ for the evaluation of its anticancer activity. The molecular mass of LYZ is 14.4 kDa and composed of 129 amino acids [19]. It is active site contains a deep crevice, which divides the protein into two separate domains linked by α helix. The first domain (residues 40–85) consists mostly of β-sheet structure, whereas the second domain (residues 89–99) is more helical in nature [20].

* Corresponding author. Tel.: +91 0661 2462284/2463284; fax: +91 0661 2462022.
E-mail address: spaul@nitrkl.ac.in (S. Paul).

http://dx.doi.org/10.1016/j.colsurfb.2015.04.017
0927-7765/

Recently, lysozyme extracted from a marine bacterium has demonstrated to inhibit angiogenesis and tumor growth in mice [21]. Lysozyme has also shown tumorigenic activity in several other studies [22].

The idea behind using LYZ to prepare self-assembled nanostructure for exploring its potential in breast cancer therapy developed from its earlier reports of antitumorigenic and anticancer potential. Caselli and Schumacher first reported the antitumorigenic activity of native lysozyme (nmLYZ) [20]. Two remarkable studies performed by Babudieri-Callerio and Callerio [23,24] demonstrated the effect of LYZ on H.S1 (mesenchymal origin), Hep2 (epithelial nature) strains and HeLa cells. The LYZ treatment produced granular irregular structures in the cytoplasm. Sava et al. in 1989 reviewed the anticancer potential of exogenous native LYZ exhaustively, where he reviewed various models and mechanism of action of LYZ-mediated cancer cell death [25]. Lysozyme was used earlier for antitumor activity in many in vivo model systems of animal tumors [26–28]. However, after 1989, except for the antiproliferative effect of recombinant human lysozyme on gastric cancer cells [29], no significant progress was made toward cancer therapeutic approach using LYZ.

Using a simple desolvation technique we have prepared self-assembled nanostructured lysozyme (snLYZ) and evaluated its possible anticancer activity. We thoroughly characterized snLYZ concerning its structure, function and stability under various stress. After a series of experimental studies, we established its strong anti-proliferative activity against breast cancer cells.

2. Materials and methods

2.1. Materials

N-acetyl-cysteine (NAC), Glutaraldehyde (25%), Tamoxifen citrate and Whatman filter paper were purchased from Sigma-Aldrich, India. Lysozyme, Bovine serum albumin, Folic acid (FA), MTT assay kit, Ethanol, DMEM, fetal bovine serum (FBS), antibiotics, DAPI, acridine orange, Fluorescein diacetate, phenylmethanesulfonyl fluoride (PMSF), Proteinase K, sodium cacodylate, sodium phosphate buffer, 1-anilinonapthalene-8-sulfonic acid and disodium EDTA were purchased from HiMedia India Pvt. Ltd. Milli Q water was used in all the experiments. T-25 flasks, 96 well plates and all other plastic wares were purchased from Tarsons, India Pvt. Ltd. 3T3 (murine fibroblast cell line), HaCaT (human keratinocyte cell line), A549 (human lung adenocarcinoma epithelial cell line) and MCF-7 (breast cancer cell line) cells were procured from NCCS, Pune, India. Triton-X was purchased from Calbiochem, India. Human blood (B +ve) was freshly obtained from the donor before the experiments. All glassware used in the study purchased from Borosil, India. All other reagents were of analytical grade.

3. Methods

3.1. Preparation of self-assembled nanostructured lysozyme (snLYZ) and its conjugates

Lysozyme (10 mg) was dissolved in 2 ml of Milli-Q water. The contents were stirred for 15 min at 500 rpm. During stirring, 8 ml of ethanol was added dropwise (1 ml/min) using an insulin syringe. After addition of ethanol, the color of the solution turns turbid white. Immediately glutaraldehyde (cross-linker) was added to achieve a final concentration of 0.1%. The contents were allowed to stir for 8 h at 500 rpm followed by 5 cycles of centrifugation (25,000 × *g*, 30 min, 40 °C). After centrifugation, the pellet was dispersed in 3 ml of Milli-Q water. The frequent washing and five cycles of centrifugation were carried out, in order to remove the residual glutaraldehyde from the formulation.

During the process of optimization, snLYZ was prepared using various concentrations of glutaraldehyde (GTD) such as 0.1%, 0.3%, 1% and 3%. The activity assay of LYZ (see Section 3.3.3), field emission scanning electron microscopy (FESEM) imaging (see Section 3.2.1), circular dichroism (CD) and tryptophan (trp) fluorescence spectroscopy (see Section 3.2.4) were performed for the optimization of GTD concentration. Although various concentration of GTD were used in the preparation of snLYZ, the optimized GTD concentration, i.e., 0.1% was used in the preparation of snLYZ and subsequent experiments.

We prepared the snLYZ-folic acid (snLYZ-FA) conjugates with the aim of increasing the specificity of snLYZ for cancer cells. For the preparation of snLYZ-FA conjugate, the prepared snLYZ was suspended in 5 ml of Milli-Q water, followed by the addition of 25 μl of 2 mg/ml stock solution of FA. The contents were stirred for 8 h at 500 rpm in the presence of 0.1% GTD. The rest of the procedure remains same as mentioned above.

The schematic representation of the whole synthesis protocol was shown in Fig. 1.

The same procedure was also followed for the preparation of self-assembled nanostructured bovine serum albumin (snBSA), a 66 kDa monomeric protein, for use as a control of snLYZ.

3.2. Characterization of prepared snLYZ

3.2.1. Field emission scanning electron microscopy (FESEM)

For capturing high-resolution images of various samples, FESEM study was performed. A volume of 10 μl of snLYZ (2 mg/ml) was spread on a glass slide and allowed to dry in a desiccator. The glass slides with the samples were fixed on a carbon tape attached to the aluminum stub. The aluminum stub was placed in a gold sputtering unit for 30 s. The samples were subsequently placed in the FESEM (NOVA NANO SEM 450) sample chamber and images were captured at a voltage of 5 kV.

3.2.2. Atomic force microscopy (AFM)

AFM imaging and measurements were performed using Bioscope Catalyst AFM (Bruker Corporation, Billerica, MA) with silicon probes. A volume of 10 μl of snLYZ (2 mg/ml) was placed on a freshly peeled mica surface followed by drying under a continuous flow of nitrogen gas. The mica discs were gently washed with 200 μl of Milli-Q water. The mica discs were allowed to dry in a desiccator overnight. The standard tapping mode was used for capturing images of different samples at room temperature in the presence of air. The nominal spring constant of the cantilever used was 20–80 N/m. A standard scan rate of 0.5 Hz with 512 samples per line was used for imaging the samples. AFM image of the snLYZ sample was captured the next day.

3.2.3. Dynamic light scattering (DLS) particle size analysis and zeta-potential analysis

The average particle size analysis and ζ-potential measurement of the aqueous suspensions of snLYZ were performed on a Malvern Zetasizer Nano-ZS DLS analyzer. A sample volume of 10 μl of snLYZ (2 mg/ml) was taken and diluted with 1990 μl of deionized water and applied to DLS for size analysis.

3.2.4. Circular dichroism (CD) and tryptophan fluorescence measurement

CD spectra of nmLYZ and snLYZ (200 μg/ml) was recorded using a JASCO J-815 CD polarimeter. Sodium cacodylate (20 mM) at pH 7.4 was used as a buffer for measuring the CD spectra. All the measurements were carried out at physiological temperature (37 °C) and a constant flow of N_2 gas. Each spectrum represented the

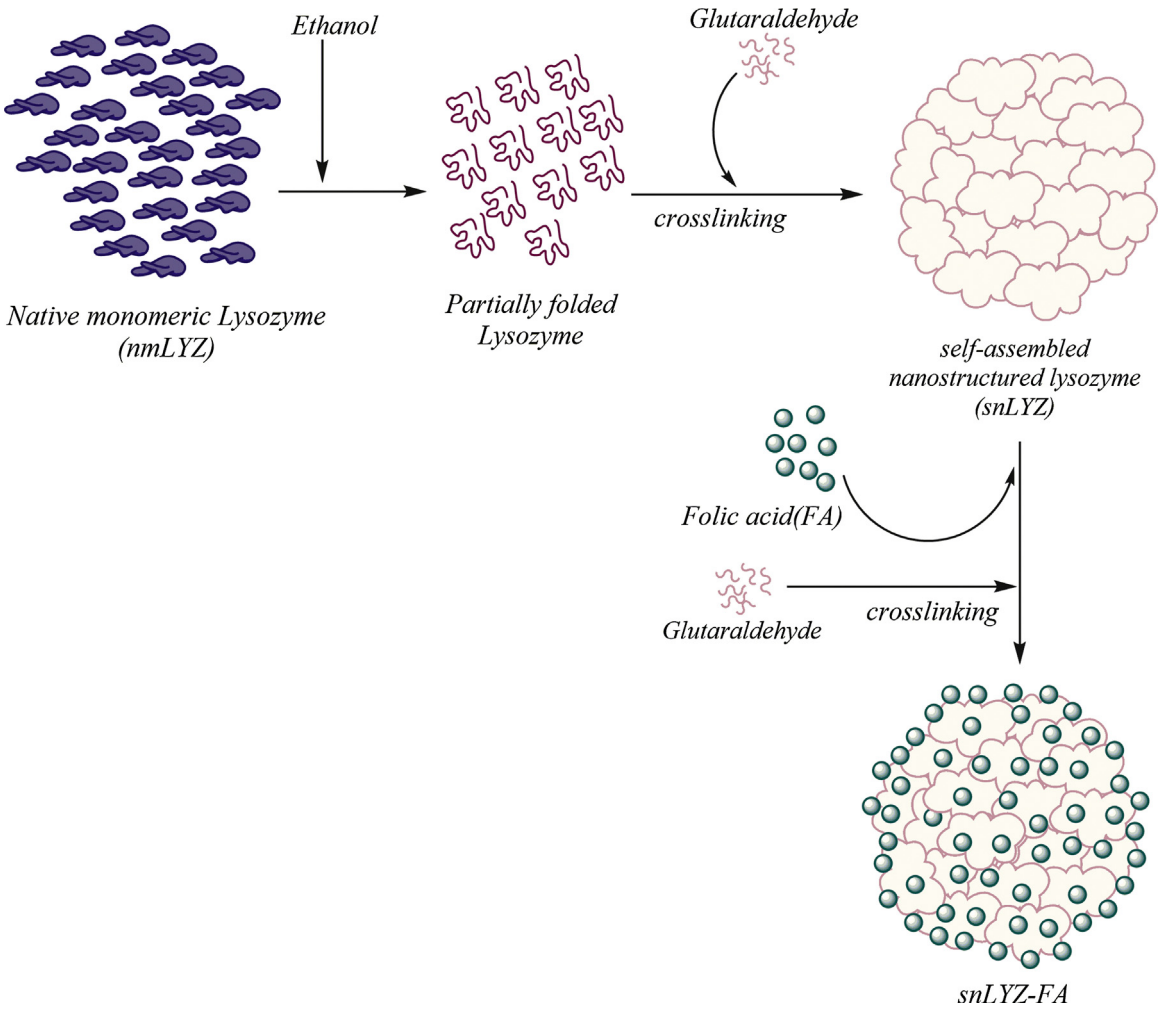

Fig. 1. Schematic representation: preparation of self-assembled nanostructured Lysozyme (snLYZ) and snLYZ-FA.

average of three accumulations recorded between wavelengths of 200 and 250 nm, with a 0.2 nm resolution, and a bandwidth of 1.0 nm. A scan speed of 100 nm/min and a standard sensitivity was set using a cuvette of path length of 0.1 cm. Appropriate buffer contribution was subtracted from every measurement. The percentage of the secondary structures (α-helix and β-sheet) was calculated using the software provided along with the instrument. The CD signal in mdeg was converted to molar residue ellipticity (θ) [deg cm^2 dmol^{-1}] using Eq. (1) [30].

$$[\theta] = \frac{100 \times \text{signal}}{C \times n \times l} \quad (1)$$

The signal is the CD output in mdeg; C represents the protein concentration in mM, 'n' represents number of amino acid residues in the protein, 'l' represents the path length in cm.

For fluorescence measurement, 20 mM sodium phosphate buffer was used at pH 7.4. The trp fluorescence spectra were measured with a Perkin-Elmer LS-55 Luminescence spectrometer. Protein samples (28 μg/ml) were incubated, and spectra were measured at 37 °C. An excitation wavelength of 290 nm was used, and trp fluorescence emission spectrum (represents the average of three accumulations recorded) of nmLYZ and snLYZ was recorded in the range of 300–400 nm. The excitation and emission slit widths were set at 5 and 10 nm, respectively. Background corrections were made with buffer without protein in all cases.

3.3. Stability analysis

3.3.1. Stability of snLYZ across various temperature and pH

Both nmLYZ and snLYZ were exposed to a temperature range of 25–80 °C using the peltier accessory and their CD spectra and fluorescence emission spectra were generated. The concentration of protein for generating CD spectra and fluorescence emission spectra were 200 μg/ml and 28 μg/ml, respectively. The secondary structural state of snLYZ was measured in a pH range of 3.0–7.4 (3, 4, 5, 6 and 7.4). The pH of the buffer was adjusted using 1.0 N hydrochloric acid. All other settings for operating the CD spectrometer and the fluorescence spectrometer remained same as mentioned in the above section.

3.3.2. Proteinase K (PK) assay

The stability of the native (nmLYZ) and self-assembled nanostructured lysozyme (snLYZ) was evaluated by analyzing the proteolytic susceptibilities of both solutions. PK (3 μM) was applied to both the solution (200 μg/ml) and incubated for 10 min. The reaction was quenched by the addition of 1 mM PMSF (PK inhibitor). The absorbance of both the samples was recorded in a wavelength range of 250–305 nm and necessary baseline corrections were made. The absorbance of the control sample, i.e., PK solution was also measured and deducted. The extent of degradation of the LYZ sample was measured from the drop in absorbance.

3.3.3. Lyz activity of snLYZ

Cells of Micrococcus lysodekticus (9 mg) were suspended in 30 ml of 100 mM sodium phosphate buffer, pH 7.4, shortly before the assay. Each of the microplate wells contained 50 μl samples and 200 μl of micrococcus cell suspension. The plate was gently shaken for 1.0 min in a microplate reader (iMark, Bio-Rad) followed by measurement of absorbance at 450 nm and continued for 10 min at 1 min interval.

To observe the effect of pH on the lytic activity of snLYZ, the pH of the sodium phosphate buffer was varied from 3 to 7.4 with the addition of 1N HCl.

Lysozyme activity [31] was measured by measuring the change in OD over a period of 10 min and is represented by the following formula.

$$\text{Lys activity (change in O.D.)} = \text{O.D.}_{\text{initial}} - \text{O.D.}_{\text{10 min}} \quad (2)$$

3.3.4. Surface hydrophobicity of snLYZ

An increase in the surface hydrophobic character of a protein has been shown to provide stability to proteins from thermal stress [32,33]. Hence, estimation of surface hydrophobic character of the protein surface will provide an indirect measurement of thermal stability of the protein. 8-Anilinonaphthalene-1-sulfonic acid (ANS) is a common extrinsic fluorescence probe usually used to determine the hydrophobic character of the protein surface. Here, snLYZ-bound ANS fluorescence was used to determine the surface hydrophobic character of the protein. ANS concentration of 110 μM was added to 6.0 μM nmLYZ and snLYZ solution prepared in 20 mM phosphate buffer, pH 7.4. Solutions were incubated for 30 min at 25 °C. Fluorescence spectra were measured with a PerkinElmer LS 55 spectrofluorimeter at 25 °C. The excitation wavelength was fixed at 350 nm with slit width 5 nm, 10 nm for excitation and emission bandpass, respectively and at a scan rate of 240 nm/min.

3.4. Cytotoxicity study of snLYZ by MTT assay

The cytotoxicity of nmLYZ and snLYZ conjugate was assessed against MCF-7 breast cancer cell line. The normal cell lines such as HaCaT (Human keratinocyte cells) and 3T3 (murine fibroblast cells) were kept as control for MTT assay. Folic acid conjugation is known to improve the uptake of various drugs [34]. Hence, folic acid was conjugated with snLYZ and the snLYZ-FA conjugate was applied to MCF-7 cells and A549 (folic acid receptor negative) lung carcinoma cells. MCF-7, HaCaT, and 3T3 cells were cultured in DMEM (Dulbecco's Minimum Essential Medium) and supplemented with 10% Foetal Bovine Serum, 2 mM glutamine and 0.1 mg/ml penicillin and streptomycin. The cells were seeded at a density of 1×10^4 cells/ml in a 96 well plate with 100 μl of DMEM in each well. The 96 well plates were maintained at 37 °C in a humidified, 5% CO_2 atmosphere in the CO_2 incubator. The cells were allowed to proliferate for 24 h. Various test samples were administered to the MCF-7 cells and the end point was monitored by MTT assay [35] at the end of next 24 h and 48 h. MTT (10 μl of 5 mg/ml stock) was added 6 h before the end point. At the end point, media was removed, and 100 μl of DMSO was added to dissolve the formazan formed and the absorbance was measured at 595 nm. The absorbance values were recorded, and percentage cell viability of MCF-7 cells was calculated from the absorbance values and the result was plotted.

It was necessary to find out, whether any other monomeric globular protein (other than lysozyme) has any cytotoxic effect in cancer cells. Hence, we performed the cytotoxicity study of snBSA against breast cancer cells MCF-7 as a control.

To examine the role of reactive oxygen species (ROS) on cell death, we applied N-acetyl-cysteine (NAC) which is a well-known inhibitor of ROS generation [32]. NAC was added to a final concentration of 2 mM in MCF-7 cell culture, and cells were allowed to proliferate as described above. After the administration of snLYZ and snLYZ-FA (conjugated with folic acid) conjugate in MCF-7 cells, MTT assay was performed at 24 and 48 h.

3.5. Cellular internalization of snLYZ observed by fluorescence microscopy

Fluorescence imaging was performed to monitor the internalization of snLYZ in MCF-7 cells using Olympus, CKX41 microscope equipped with a fluorescence attachment. The cells were seeded at a density of 1×10^4 cells/ml and allowed to grow for 24 h. At the end of 24 h, media was replaced, the fluorescence image of MCF-7 cells was taken, and immediately snLYZ cross-linked with acridine orange fluorescent probe, was added. At the end of 1 h, one batch of cells were washed with 5 ml of PBS pH 7.4 followed by the addition of Fluorescein diacetate and DAPI for staining the cells. The above process was repeated for respective batch of cells at 3, 6 and 12 h post-administration. Imaging of cancer cells were carried out at 400× magnification.

3.6. Hemocompatibility assay

Human blood (5 ml) was collected by an expert technician under the supervision of an invited physician. Blood was collected in a centrifuge tube containing 2 mg of disodium EDTA (anti-coagulant). The contents were gently resuspended and centrifuged at $1000 \times g$ for 10 min. The supernatant was removed and the RBC collected at the bottom of the centrifuge tube was washed three times by gentle resuspension with 10 times the volume of pyrogen-free saline (0.9% NaCl) and followed by centrifugation at $1000 \times g$ for 10 min at room temperature. The RBC pellet was gently resuspended in saline and was diluted to 0.8% (v/v). The suspended RBC solution (3 ml) was placed in sterile glass vials, and various test samples were added to evaluate their hemolytic potential. Triton X (1%) was used as a positive control for monitoring maximum hemolysis and RBC suspension treated with normal saline was used as a negative control. The absorbance at 405 nm was measured as an indicator of hemoglobin released into the supernatant. The percentage hemolysis was calculated at 1 h, and the graph was plotted between percent hemolysis and time (h).

3.7. Statistical analysis

Data were presented as mean ± S.E.M. The statistical analysis were carried out by One-way ANOVA followed by Tukey's test using Graph Pad Prism 5.0 software.

4. Results and discussion

4.1. Preparation of self-assembled nanostructured lysozyme (snLYZ) and its conjugates

We used GTD as a cross linker for the preparation of self-assembled nanostructured Lysozyme (snLYZ). Since the particle is a protein, the addition of GTD could induce a change in its structure and function apart from allowing the partially folded protein molecules to a self-assembled state in an ordered manner. By measuring the LYZ activity, as well as the drop in trp fluorescence intensity, we optimized the GTD concentration for the preparation of snLYZ.

During optimization of GTD concentration, we used various concentrations of GTD (0.01%, 0.05%, 0.1%, 0.3%, 1.0% and 3.0%) for estimation of LYZ biological activity of the prepared snLYZ (Fig. S1, supplementary data). The enzyme activity of snLYZ prepared using 0.1% GTD showed a substantial reduction of ~28.5%. A similar

level of drop in LYZ activity in snLYZ samples prepared with 0.01% and 0.05% GTD (Fig. S1, supplementary data) was also observed. We also measured the trp fluorescence for the optimization of GTD concentration, toward the preparation of snLYZ. Varying concentrations of GTD were added to the solution of nmLYZ, followed by 1 h incubation. After incubation, we measured the trp fluorescence to monitor any conformational change that took place around trp of nmLYZ. Fig. S2A (supplementary data) shows the drop in trp fluorescence intensity that indirectly indicates the change of environment around trp. We observed that 0.1% GTD triggered a change in the trp environment in nmLYZ to an extent higher than 0.01% and 0.05% GTD-treated nmLYZ samples. However, we also observed that GTD concentration beyond 0.1% caused substantial trp fluorescence reduction, i.e., higher conformational perturbance around trp residues. CD spectra were also measured to investigate the trend of secondary structural change concerning various GTD concentrations (Fig. S2B, supplementary data). No significant change in CD signal (in molar ellipticity (θ) (deg cm^2 dmol^{-1}) was observed up to 0.3% GTD. However, a change was observed when GTD was used in nmLYZ above 0.3% such as 0.5% and 1.0%. Hence, we concluded to use 0.1% GTD in the preparation of snLYZ and characterized further.

We also used 0.01% and 0.05% GTD in the preparation of snLYZ. However, we found the crosslinking was insufficient to provide a stable structure as it resulted in the formation of disordered assemblies of LYZ (result not shown). Use of higher concentration of GTD such as 0.3%, 1% and 3% caused the production of large sized assemblies (Fig. S3A–C supplementary data) due to excessive number of cross linkages. Moreover, it might result in the suppression of inherent biological function and structural integrity of LYZ due to excessive accumulation of GTD throughout the protein backbone and surface.

4.2. Characterization of prepared snLYZ

FESEM image of snLYZ prepared with 0.1% GTD shows high homogeneity in size (300–400 nm) and shape (Fig. 2A). Atomic force microscopy (AFM) image also revealed the average size of snLYZ close to 300 nm (Fig. 2B). From Fig. 2C, the average size of snLYZ was found to be approximately 300 nm, which is also in agreement with the size obtained from the FESEM and AFM images. The size of prepared snBSA was 800 nm and spherical in shape (see Fig. S9, supplementary figure). Moreover, one of the most important aspects of our result was the shape of snLYZ particles, which was clearly observed to be spherical. Such spherical shape offers least resistance against the flow and achieves maximum penetration potential across cell membranes.

The zeta potential of snLYZ was found to be −39.1 mV. Zeta potential usually measures the electrostatic potential at the surface of the particle. Normally ±30 mV suggests that the particles in suspension are highly stable and less susceptible to agglomeration.

Since the protein was self-assembled to form snLYZ, it was necessary to know the change of its conformation specifically secondary structural components such as α-helix and β-sheet. Fig. 2D, clearly showed a drastic reduction in CD signal of snLYZ, due to the destruction of secondary structures of the protein resulting in the significant percentage increase in β-sheet content. The trp fluorescence spectra (Fig. 2E) also revealed a clear drop in trp fluorescence intensity for snLYZ. The result clearly indicates that trp

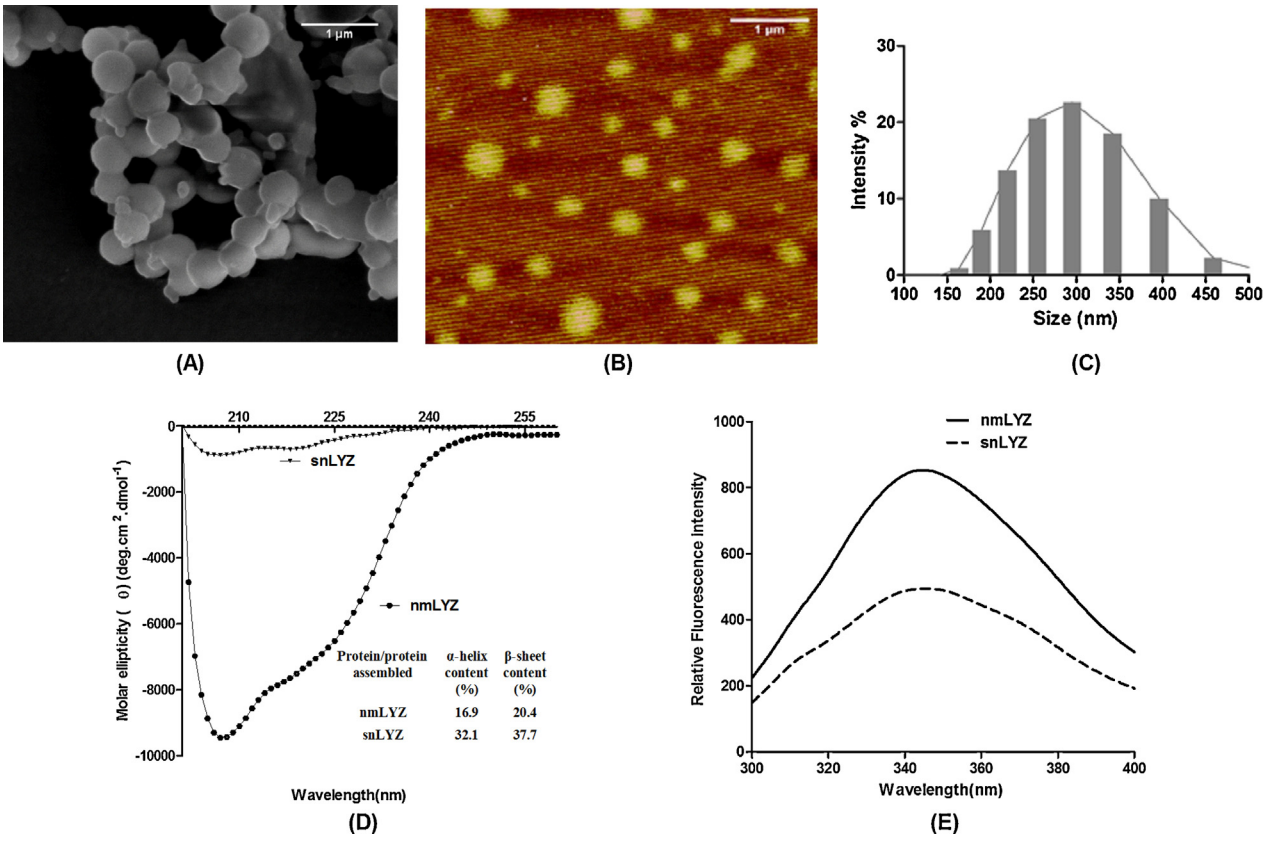

Fig. 2. FESEM image of snLYZ prepared using 0.1% GTD as a cross linker (B) AFM image of snLYZ. (C) DLS particle size analysis of snLYZ. (D) Circular dichroism spectra of nmLYZ and snLYZ. The inset data shows the percentage of secondary structural components calculated using the software associated with the instrument. (E) trp fluorescence spectra of nmLYZ and snLYZ. All data were expressed as mean of three readouts generated from the instrument for (D) and (E).

residues moved from their original location (in nmLYZ) to a more polar environment and perhaps exposed to the surface.

4.3. Stability analysis under various temperature conditions

We also wanted to investigate the thermal stability of the samples in a temperature range of 25–80°C. Since the physiological temperature is considered to be 37 °C, we monitored the conformational state of samples below and above the physiological temperature (Fig. S4A, supplementary data) showed the plot of fluorescence intensity at 345 nm against temperature, which clearly indicates that snLYZ was more stable than nmLYZ since it has a relatively lower drop in fluorescence intensity. We also plotted the CD signal (molar ellipticity (θ) deg cm^2 dmol^{-1}) at 222 nm vs. temperature (Fig. S4B, supplementary data) which is associated with the α-helical content. The plot indicated that there was almost no change in α helical structure with temperature, but significant change observed in nmLYZ. CD results (Fig. S4C, supplementary data) revealed significant amount change in CD signal of nmLYZ but not in snLYZ. Such high stability was due to high β-sheet contents in snLYZ. Therefore, both the CD and fluorescence results established the conformational stability of snLYZ in a wide range of temperature for storage, handling and use of snLYZ.

4.4. Stability of snLYZ under varying pH

It was essential to examine the stability of prepared snLYZ under various stresses like pH and Proteinase K (PK). Fig. S4D (supplementary data) presented the plot of the lytic activity of LYZ in snLYZ vs. pH, which revealed a very minimal change in the lytic activity of snLYZ in a range of pH 5.0–9.0. However, nmLYZ showed a drastic drop in activity toward higher pH starting from pH 5.0, with a maximum drop at pH 9.0. CD signal measured at 222 nm demonstrated an insignificant change in α helical component (Fig. S4E, supplementary data). The intrinsic fluorescence measurement clearly showed an insignificant change in trp fluorescence (Fig. S4F, supplementary data) of snLYZ, compared to nmLYZ.

4.5. Stability of snLYZ against Proteinase K

PK-mediated digestion study was also performed to understand the resistance against protease digestion. PK normally digests non-native proteins very fast but not the native one. The high amount of PK can also attack native structure as well. In this case, nmLYZ was native but snLYZ was partially denatured as well as partly unfolded but self-assembled by crosslinking with 0.1% GTD. After PK digestion, spectroscopic measurement of snLYZ showed almost no change in the peak of spectra indicating increased stability against PK digestion compared to nmLYZ (Fig. S4G and H supplementary data). Necessary baseline correction was done in order to compare the plots.

The above result also indicates a possibility that in snLYZ, the digestion sites were perhaps not well accessible to PK due to the self-assembly process of nmLYZ. Moreover, such stability both against pH and PK might be due to higher contents of β-sheet (37.7%) in snLYZ (Fig. 2D) than nmLYZ. All of the above collectively led to the conclusion that snLYZ might be considered to be structurally, functionally and biologically stable which satisfies one of the most essential requirements for a drug.

4.6. Assessment of surface hydrophobic character of snLYZ using ANS fluorescence

The thermal stability of a protein is also positively correlated with its higher surface hydrophobic character. Hence, measuring the surface hydrophobicity of snLYZ and nmLYZ can throw light on the stabilizing effect. ANS is an anionic, aliphatic fluorescence dye that spontaneously interacts with non-polar surface residues of a protein and exhibit strong fluorescence. Hence, measuring the ANS bound fluorescence will provide information about the surface hydrophobicity of snLYZ. From our results (Fig. S4I, supplementary data), it was clear that our prepared snLYZ demonstrated higher hydrophobic surface (as reflected by a higher amount of snLYZ bound ANS fluorescence) than nmLYZ-bound fluorescence. Hence, we concluded that more non-polar residues were relocated on the surface of snLYZ that also support our previous data obtained from trp fluorescence spectroscopy (Fig. 2E).

4.7. Cytotoxicity study of snLYZ

The cytotoxicity assay of nmLYZ and snLYZ was performed against human breast cancer cells MCF-7. Results showed that the administration of nmLYZ caused insignificant cancer cell killing compared to control (administered with none) till a dose of 200 μg/ml. However, snLYZ demonstrated a dose-dependent cell killing with more than 90% cell death at 200 μg/ml of snLYZ after 24 h administration (Fig. 3A). Surprisingly, when cell killing was measured after 48 h of snLYZ administration, almost complete (∼98% with ±1.8% error) cell killing was found at a snLYZ dose of 200 μg/ml. At a lower dose like 60 and 100 μg/ml, the death was found to be ∼95% and 96%, respectively (Fig. 3B), proved its strong anti-proliferative activity. Tamoxifen (TAM), a chemotherapeutic agent used in breast cancer, was also used here as a positive control for comparison (Fig. S5B, supplementary data). The complete dose-dependent anti-proliferative effect of nmLYZ and snLYZ was shown in Fig. S5A, supplementary data. To test whether protein nanoparticle is specific to cancer cells, we performed cytotoxicity study against human keratinocyte cells HaCaT and mouse fibroblast cells 3T3. The results clearly showed that snLYZ did not show cytotoxicity against HaCaT as well as 3T3 cells (see supplementary Fig. S8). The cytotoxicity study of snBSA in MCF-7 and 3T3 cells clearly revealed that snBSA, could not produce cytotoxicity in cancer cells as well as normal murine fibroblast cells 3T3 (see supplementary Fig. S10A and B). The snBSA was prepared using the same experimental protocol as that of snLYZ. The result also confirms the specific cytotoxicity of snLYZ for cancer cells.

We also administrated 0.1% and 0.2% GTD in the cell culture medium as a control to observe its cytotoxic effect in both MCF-7 and 3T3 cells. We did not find any toxic effect of GTD at such concentrations both in breast cancer cells MCF-7 and normal murine fibroblast 3T3 cells (Fig. S10A and B).

In order to understand the cell death mechanism mediated by snLYZ, we administered N-acetyl-L-cysteine (NAC) in cell culture medium to examine the possibility of cell death caused by reactive oxygen species (ROS). NAC is an antioxidant/free-radical scavenger or reducing agent that protects cells against ROS-mediated death [32]. In our investigation, NAC (2 mM) was used to inhibit ROS-based effect. The idea was if NAC was administered in the cell medium, ROS generation would be inhibited and cell killing induced by ROS would be prevented. From Fig. 3A, it was found that snLYZ at a concentration of 60, 100 and 200 μg/ml shows 34.09%, 22.27% and 8.27% cell viability respectively. However, administration of NAC (2 mM) caused almost no cell death, clearly indicating a complete ROS-mediated cancer cell death mechanism by snLYZ.

In order to increase the specificity of snLYZ toward MCF-7 cells, we also conjugated folic acid (FA) with snLYZ. We observed higher cell killing by snLYZ-FA than snLYZ (Fig. 3C and D). We anticipated that the increase in cytotoxicity might be due the presence of FA receptors present on the MCF-7 cell surface. The receptors facilitated the internalization of snLYZ-FA by receptor-mediated

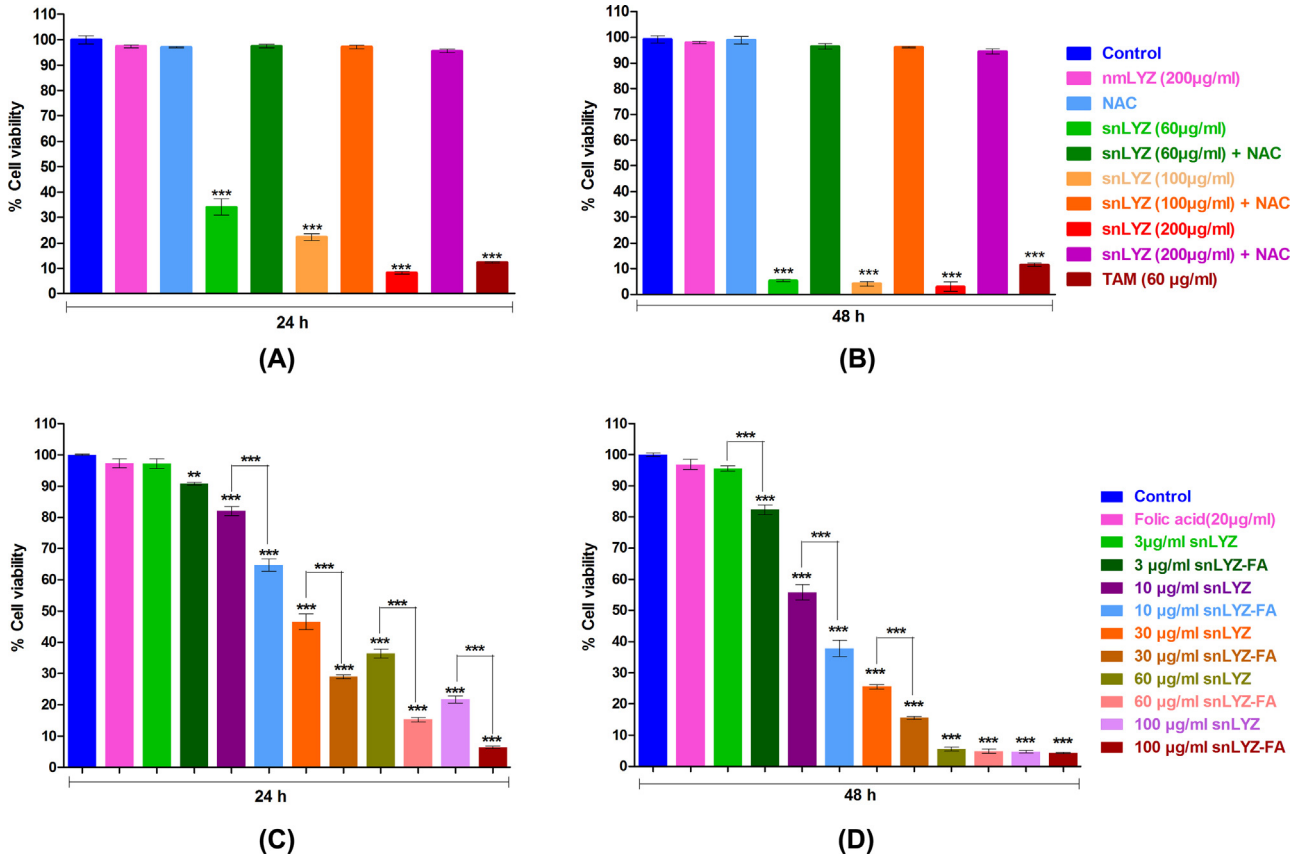

Fig. 3. Cytotoxicity study by MTT assay on MCF-7 cells. (A) Effect of NAC on snLYZ at 24 h post administration. (B) Effect of NAC on snLYZ at 48 h post administration. (C) snLYZ-FA at 24 h post administration. (D) snLYZ-FA at 48 h post administration. Statistically significant vs. control group, $^{**}p < 0.01$, $^{***}p < 0.001$ by One way ANOVA and post Tukey test. All data are expressed as mean ± S.E.M, $n = 3$.

endocytosis. In order to observe the effect of snLYZ-FA on cells that do not express folic acid receptors, we performed cell viability studies in A549 cells. We found reduced cytotoxicity of snLYZ-FA in A549 cells (see Fig. S11, supplementary figure) compared to MCF-7 cells (see Fig. 3C). The result clearly indicates that folic acid expressing cancer cells are more susceptible to the cytotoxicity of snLYZ-FA, compared to cancer cells that do not express folate receptors.

We also observed partial loss of biological activity of LYZ in snLYZ compared to nmLYZ, however with a multi-fold gain in cancer cell killing potential. This fact clearly proved that the lytic activity of LYZ has no role in the cancer cell-killing mechanism.

4.8. Cellular uptake of snLYZ

To ascertain the cellular uptake of snLYZ, we performed fluorescence imaging of cancer cells using fluorescent dyes such as DAPI, Fluorescein diacetate, and acridine orange. Cells stained with DAPI clearly showed blue fluorescence for the nucleus in live cells and Fluorescein diacetate exhibited green fluorescence for the cytoskeletal component of cells. Cancer cells at 0th h were presented in Fig. 4(A–E), which showed the intact nucleus (blue fluorescence) with uniform cytoskeletal components and intact boundary of cells. Fig. 4(A–Y) clearly showed that with an increase in time (1–12 h), more amount of snLYZ was internalized in cancer cells resulting in the formation of cytoplasmic granules causing damage to the cell membrane.

Babudieri-Callerio reported that native LYZ (0.1–5 mg/ml) upon administration in human tumorigenic cell lines resulted in the formation of many azurophilic granules in the cytoplasm (diameter ~1 μm). The result was anticipated as one of the reason behind LYZ-based cell death [21]. Here, a similar kind of granular formation was also observed (Fig. 4F, K, P, and U). Subsequently, the same group reported that the generation of the granular structure within the cytoplasm was due to the interaction of lysozyme with the endoplasmic reticulum membrane. The interaction occurred through an enzymatic mechanism involving homogenization of its fibrillar structure [22]. In this study, we observed similar interaction, which resulted in overwhelming ROS production and triggered profound cell death.

Moreover, the appearance of the damaged cytoplasmic membrane with intact and slightly swollen nucleus (Fig. 4T), is indicative of cellular necrosis. Interestingly, the granular formation within the cytosol seemed to initiate the cytosolic damage. Accordingly, after entering into cells, snLYZ caused cytosolic damage and increased permeability of the cellular membrane.

Rammer et al. recently demonstrated that BAMLET kills MCF-7 cells by activating a lysosomal cell death mechanism involving leakage of lysosomal cathepsin into the cytoplasm followed by activation of the pro-apoptotic protein Bax [17]. Here, we demonstrate a similar mechanistic trend where initially cytosolic bodies were damaged, whereas the nucleus remained intact, much like the cathepsin-induced necrotic cell death. In other findings, Hoque and his colleagues recently documented that oleic acid and bovine α-lactalbumin complex (BAMLET) was hemolytic to human, goat and buffalo erythrocytes. Here, oleic acid played the key role in killing tumor cells, which had hemotoxicity [36]. Therefore, in our study we wanted to evaluate the biocompatibility of snLYZ to human erythrocytes.

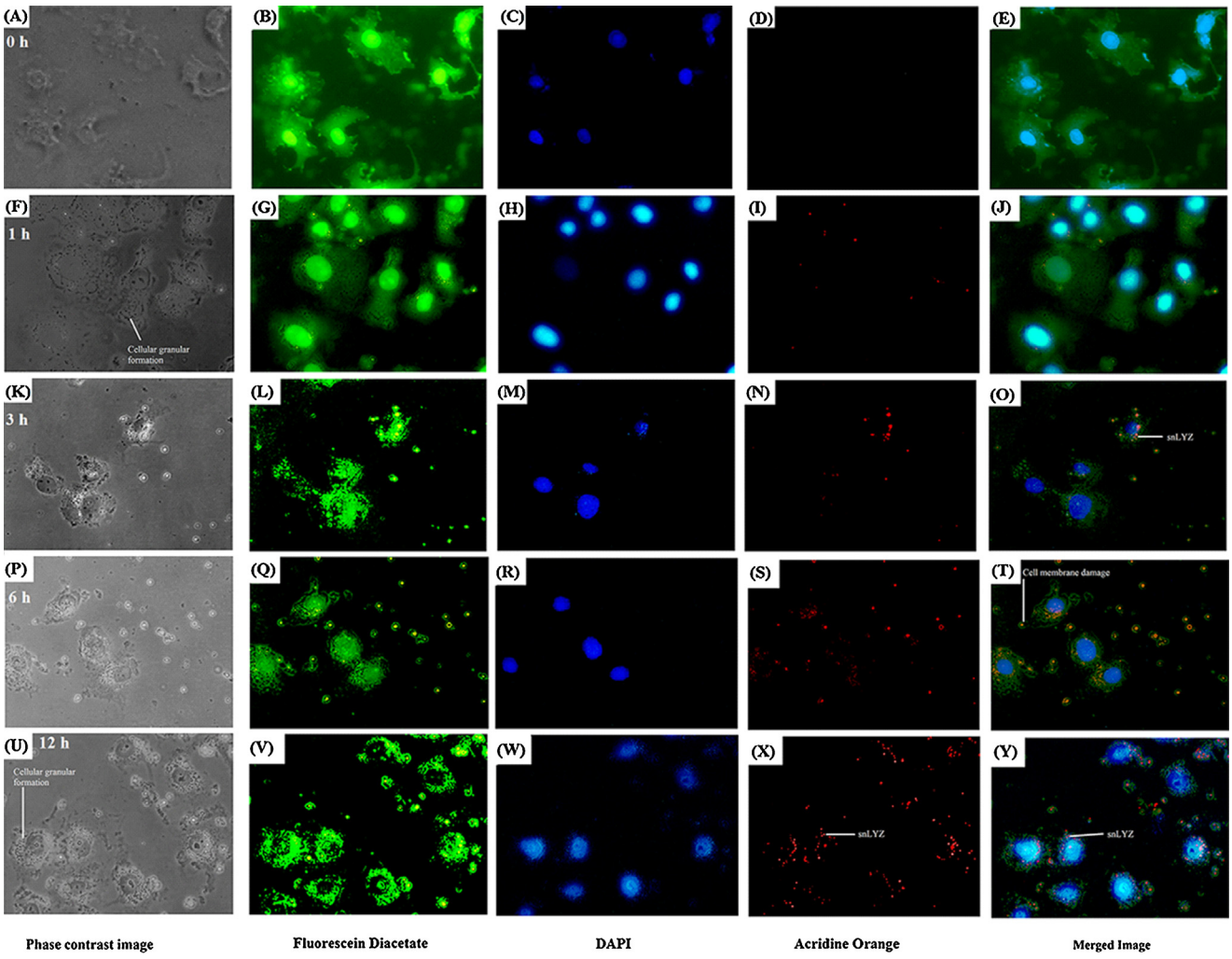

Fig. 4. Fluorescent images of MCF-7 cancer cells showing internalization of acridine orange tagged snLYZ. (A–E) control, administered with none; (F–J) cell images after administration of acridine orange tagged snLYZ uptake for 1 h; (K–O) acridine orange tagged snLYZ uptake at 3 h; (P–T) acridine orange tagged snLYZ uptake at 6 h; (U–Y) acridine orange tagged snLYZ uptake at 12 h. The black spot-like structures present within the cytoplasm were marked as granules. (For interpretation of the references to color in this text, the reader is referred to the web version of the article.)

4.9. Hemolysis assay

Although we have already established that snLYZ triggers cell killing through cellular internalization, its hemocompatibility nature has yet not been analyzed. Since snLYZ is a proteinaceous material, it was expected that it should not cause any toxicity to healthy cells like erythrocytes. However, such effect must be examined. Hemolysis assay was performed as per the protocol mentioned in Section 3.6. Since our earlier experimental results already showed that TAM had higher cancer cell-inhibitory potential than snLYZ, we also simultaneously examined the hemotoxicity of TAM. Our objective was to assess the possibility of using snLYZ as a potential breast cancer therapeutic agent for human use and in order to examine that it was essential to study its hemocompatible property.

Fig. S6 (see the supplementary figure) showed the hemolytic propensity of various formulations. It was clear from the results that snLYZ showed negligible hemolytic potential compared to TAM. The reason behind the hemocompatible nature of snLYZ was due to its proteinaceous composition and hence, it can only be administered intravenously so that it can reach the site of cancer in the body without being digested. In Fig. S7 (supplementary figure), we proposed a model of how our developed snLYZ might have killed cancer cells efficiently.

Although snLYZ caused insignificant level of hemolysis which indicates that it is not harmful to normal cells like erythrocytes, it caused a rapid ROS-dependent cancer cell death. The result suggests that snLYZ prevents the cancer cell-specific mechanism of counteracting additional ROS generation, perhaps through extra antioxidant production. Liu et al. earlier demonstrated that LYZ ameliorated oxidative stress in normal cells. LYZ by binding to agents such as advanced glycation end products (AGE) generated ROS using its unique 18 amino acid domain [37]. It is plausible that in snLYZ, such domain function was diminished due to conformational changes which further reverted to a partially unfolded state that suppressed the extra antioxidant generation mechanism in cancer cells.

5. Conclusion

The structure and the biological function of cellular proteins are intimately linked. Proteins have been considered to be the promising biomolecules in various areas of biology and medicine. However, their use has been restricted due to their structural and functional sensitivity toward various kinds of stresses, such as the pH and, temperature, which limit their application as drugs or pharmaceutical carriers. Therefore, in order to design them for the use as biomaterials and biomedicines, the above limitations must be

overcome. In the present communication, we have reported for the first time that lysozyme protein can be made lethal to breast cancer cells by preparing its self-assembled nanostructure particles. Here, we developed a stable self-assembled nanostructured lysozyme-based particle (snLYZ) that proved to be highly biocompatible and suitable for a possible therapy of breast cancer. However, our nanostructured protein agents should also be explored in other types of cancers. Moreover, our prepared snLYZ can further be explored in areas like tissue engineering and regenerative medicines as a suitable biomaterial.

Acknowledgements

We sincerely acknowledge the support provided by Department of Biotechnology (DBT), Department of Science and Technology (DST), Govt. of India and National Institute of Technology Rourkela, Govt. of India for carrying out this work. The authors gratefully acknowledge Dr. A. J. Lakhter for critical proofreading of the manuscript.

Appendix A. Supplementary data

Supplementary data associated with this article can be found, in the online version, at http://dx.doi.org/10.1016/j.colsurfb.2015.04.017

References

[1] J.M. Thornton, C.A. Orengo, A.E. Todd, F.M. Pearl, Protein folds, functions and evolution, J. Mol. Biol. 293 (1999) 333–342.
[2] H. Hegyi, M. Gerstein, The relationship between protein structure and function: a comprehensive survey with application to the yeast genome, J. Mol. Biol. 288 (1999) 147–164.
[3] A.C.R. Martin, C.A. Orengo, E.G. Hutchinson, S. Jones, M. Karmirantzou, R.A. Laskowski, J.B.O. Mitchell, C. Taroni, J.M. Thornton, Protein folds and functions, Structure 6 (1998) 875–884.
[4] C.A. Ross, M.A. Poirier, Protein aggregation and neurodegenerative disease, Nat. Med. 10 (Suppl.) (2004) S10–S17.
[5] A. Aguzzi, T. O'Connor, Protein aggregation diseases: pathogenicity and therapeutic perspectives, Nat. Rev. Drug Discov. 9 (2010) 237–248.
[6] M. Jucker, L.C. Walker, Self-propagation of pathogenic protein aggregates in neurodegenerative diseases, Nature 501 (2013) 45–51.
[7] P. Ciryam, G.G. Tartaglia, R.I. Morimoto, C.M. Dobson, M. Vendruscolo, Widespread aggregation and neurodegenerative diseases are associated with supersaturated proteins, Cell Rep. 5 (2013) 781–790.
[8] S. Zhang, Fabrication of novel biomaterials through molecular self-assembly, Nat. Biotechnol. 21 (2003) 1171–1178.
[9] A. Gangar, A. Fegan, S.C. Kumarapperuma, P. Huynh, A. Benyumov, C.R. Wagner, Targeted delivery of antisense oligonucleotides by chemically self-assembled nanostructures, Mol. Pharm. 10 (2013) 3514–3518.
[10] E. Jabbari, Targeted delivery with peptidomimetic conjugated self-assembled nanoparticles, Pharm. Res. 26 (2009) 612–630.
[11] S.D. Li, Y.C. Chen, M.J. Hackett, L. Huang, Tumor-targeted delivery of siRNA by self-assembled nanoparticles, Mol. Ther. 16 (2008) 163–169.
[12] Y. Liu, J. Sun, W. Cao, J. Yang, H. Lian, X. Li, Y. Sun, Y. Wang, S. Wang, Z. He, Dual targeting folate-conjugated hyaluronic acid polymeric micelles for paclitaxel delivery, Int. J. Pharm. 421 (2011) 160–169.
[13] J.J. Panda, A. Varshney, V.S. Chauhan, Self-assembled nanoparticles based on modified cationic dipeptides and DNA: novel systems for gene delivery, J. Nanobiotechnol. 11 (2013) 18.
[14] X. Xu, Y. Jian, Y. Li, X. Zhang, Z. Tu, Z. Gu, Bio-inspired supramolecular hybrid dendrimers self-assembled from low-generation peptide dendrons for highly efficient gene delivery and biological tracking, ACS Nano 8 (2014) 9255–9264.
[15] G. Zhu, J. Zheng, E. Song, M. Donovan, K. Zhang, C. Liu, W. Tan, Self-assembled, aptamer-tethered DNA nanotrains for targeted transport of molecular drugs in cancer theranostics, Proc. Natl. Acad. Sci. U. S. A. 110 (2013) 7998–8003.
[16] C. Weber, C. Coester, J. Kreuter, K. Langer, Desolvation process and surface characterisation of protein nanoparticles, Int. J. Pharm. 194 (2000) 91–102.
[17] P. Rammer, L. Groth-Pedersen, T. Kirkegaard, M. Daugaard, A. Rytter, P. Szyniarowski, M. Hoyer-Hansen, L.K. Povlsen, J. Nylandsted, J.E. Larsen, M. Jaattela, BAMLET activates a lysosomal cell death program in cancer cells, Mol. Cancer Ther. 9 (2010) 24–32.
[18] M. Zhang, F. Yang Jr., F. Yang, J. Chen, C.Y. Zheng, Y. Liang, Cytotoxic aggregates of alpha-lactalbumin induced by unsaturated fatty acid induce apoptosis in tumor cells, Chem. Biol. Interact. 180 (2009) 131–142.
[19] R.E. Canfield, The amino acid sequence of egg white lysozyme, J. Biol. Chem. 238 (1963) 2698–2707.
[20] P. Caseli, H. Schumacher, Inhibizione dello sviluppo del sarcoma di Rous nella cornea e nel derma di pollo a mezzo di proteine basiche, Boll. Ocul. 34 (1955) 513–533.
[21] J. Ye, C. Wang, X. Chen, S. Guo, M. Sun, Marine lysozyme from a marine bacterium that inhibits angiogenesis and tumor growth, Appl. Microbiol. Biotechnol. 77 (2008) 1261–1267.
[22] G. Sava, A. Benetti, V. Ceschia, S. Pacor, Lysozyme and cancer: role of exogenous lysozyme as anticancer agent (review), Anticancer Res. 9 (1989) 583–591.
[23] C. Callerio, Appearance of granules in the cytoplasm of tumour-cell cultures in contact with lysozyme, Nature 184 (1959) 202–203.
[24] D. Callerio-Babudieri, C. Callerio, Electron microscope observations of tumour cell cultures in the presence of lysozyme, Nature 200 (1963) 693–694.
[25] G. Sava, L. Perissin, S. Zorzet, C. Callerio, Antineoplastic effects of egg-white lysozyme in mice bearing solid metastasizing tumors, Anticancer Res. 6 (1985) 183–186.
[26] K. Fukawa, N. Nishimura, O. Irino, K. Nakazato, A. Taguchi, K. Nitta, Experimental studies on antitumor effects of lysozyme, Gan To Kagaku Ryoho 9 (1982) 915–923.
[27] G. Sava, Reduction of B16 melanoma metastases by oral administration of egg-white lysozyme, Cancer Chemother. Pharmacol. 25 (1989) 221–222.
[28] G. Sava, L. Perissin, S. Zorzet, Antimetastatic action of orally administered lysozyme in mice bearing Lewis lung carcinoma, Clin. Exp. Metastasis 6 (1988) 245–253.
[29] T.K. Guo, X. Zhao, X.D. Xie, Z.H. Chen, C.S. Zhou, L.L. Wei, H. Zhang, The anti-proliferative effects of recombinant human lysozyme on human gastric cancer cells, J. Int. Med. Res. 35 (2007) 353–360.
[30] C.D. Sohl, E.M. Isin, R.L. Eoff, G.A. Marsch, D.F. Stec, F.P. Guengerich, Cooperativity in oxidation reactions catalyzed by cytochrome p450 1A2 highly cooperative pyrene hydroxylation and multiphasic kinetics of ligand binding, J. Biol. Chem. 283 (2008) 7293–7308.
[31] A. Ng, M. Heynen, D. Luensmann, L.N. Subbaraman, L. Jones, Optimization of a fluorescence-based lysozyme activity assay for contact lens studies, Curr. Eye Res. 38 (2013) 252–259.
[32] M.M. Gromiha, M.C. Pathak, K. Saraboji, E.A. Ortlund, E.A. Gaucher, Hydrophobic environment is a key factor for the stability of thermophilic proteins, Proteins 81 (2013) 715–721.
[33] C.N. Pace, H. Fu, K.L. Fryar, J. Landua, S.R. Trevino, B.A. Shirley, M.M. Hendricks, S. Iimura, K. Gajiwala, J.M. Scholtz, G.R. Grimsley, Contribution of hydrophobic interactions to protein stability, J. Mol. Biol. 408 (2011) 514–528.
[34] F. Wang, Y. Chen, D. Zhang, Q. Zhang, D. Zheng, L. Hao, Y. Liu, C. Duan, L. Jia, G. Liu, Folate-mediated targeted and intracellular delivery of paclitaxel using a novel deoxycholic acid-O-carboxymethylated chitosan-folic acid micelles, Int. J. Nanomed. 7 (2012) 325–337.
[35] T. Mosmann, Rapid colorimetric assay for cellular growth and survival: application to proliferation and cytotoxicity assays, J. Immunol. Methods 65 (1983) 55–63.
[36] M. Hoque, S. Dave, P. Gupta, M. Saleemuddin, Oleic acid may be the key contributor in the BAMLET-induced erythrocyte hemolysis and tumoricidal action, PLoS ONE 8 (2013) e68390.
[37] H. Liu, F. Zheng, Q. Cao, B. Ren, L. Zhu, G. Striker, H. Vlassara, Amelioration of oxidant stress by the defensin lysozyme, Am. J. Physiol. Endocrinol. Metab. 290 (2006) E824–E832.